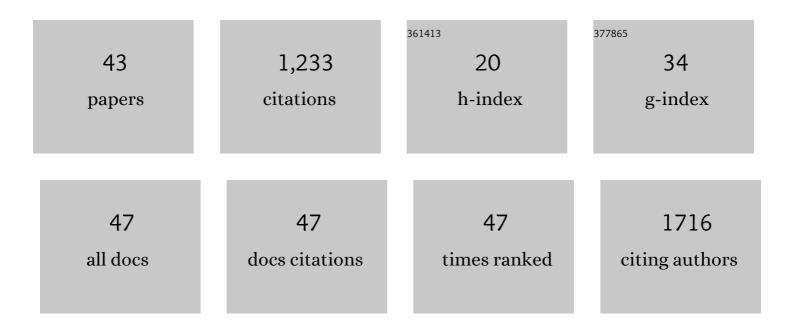


List of Publications by Year in descending order

Source: https://exaly.com/author-pdf/9087759/publications.pdf Version: 2024-02-01



ARTICLE IF CITATIONS CRISPR-Cas12a-regulated DNA adsorption and metallization on MXenes as enhanced enzyme mimics for sensitive colorimetric detection of hepatitis B virus DNA. Journal of Colloid and Interface Ścience, 9.4 2022, 613, 406-414. Reduced intracellular chloride concentration impairs angiogenesis by inhibiting oxidative 9 6.1 7 stress-mediated VEGFR2 activation. Acta Pharmacologica Sinica, 2021, 42, 560-572. Intra-Procedural CT/MR-Ultrasound Fusion Imaging Helps to Improve Outcomes of Thermal Ablation 1.5 for Hepatocellular Carcinoma: ResultsÂin 502 Ňodules. Ultraschall in Der Medizin, 2021, 42, e9-e19. Dynamic Contrast-Enhanced Ultrasound Radiomics for Hepatocellular Carcinoma Recurrence 4 2.6 24 Prediction After Thermal Ablation. Molecular Imaging and Biology, 2021, 23, 572-585. Utility of Fusion Imaging for Percutaneous Thermal Ablation of Hepatocellular Carcinoma in the Caudate Lobe. Journal of Vascular and Interventional Radiology, 2021, 32, 1209-1214. Thermal ablation of medium-sized hepatocellular carcinomas using intraoperative ultrasound fusion 6 imaging: A propensity score-matched analysis. Clinics and Research in Hepatology and 1.5 3 Gastroenterology, 2021, 45, 101581. ILF3 is a substrate of SPOP for regulating serine biosynthesis in colorectal cancer. Cell Research, 48 2020, 30, 163-178. In-depth mapping carboxylic acid metabolome reveals the potential biomarkers in colorectal cancer 8 5.4 17 through characteristic fragment ions and metabolic flux. Analytica Chimica Acta, 2020, 1128, 62-71. Value of artificial ascites to assist thermal ablation of liver cancer adjacent to the gastrointestinal 2.6 tract in patients with previous abdominal surgery. BMC Cancer, 2020, 20, 763. Transcholecystic Contrast-Enhanced Ultrasound-Guided Percutaneous Transhepatic Biliary Drainage 10 for Central Bile Duct Protection During Thermal Tumor Ablation. Journal of Vascular and 0.5 1 Interventional Radiology, 2020, 31, 1587-1591. A review of thyroid gland segmentation and thyroid nodule segmentation methods for medical 4.7 ultrasound images. Computer Methods and Programs in Biomedicine, 2020, 185, 105329. Mesenchymal stem cells promote human melanocytes proliferation and resistance to apoptosis 12 5.5 23 through PTEN pathway in vitiligo. Stem Cell Research and Therapy, 2020, 11, 26. One-lung ventilation for percutaneous thermal ablation of liver tumors in the hepatic dome. 2.5 International Journal of Hyperthermia, 2020, 37, 49-54. CSN6–TRIM21 axis instigates cancer stemness during tumorigenesis. British Journal of Cancer, 2020, 14 6.4 19 122, 1673-1685. Intraprocedural contrast-enhanced ultrasound-CT/MR fusion imaging assessment in HCC thermal ablation to reduce local tumor progression: compared with routine contrast-enhanced ultrasound. International Journal of Hyperthermia, 2019, 36, 784-792. Microwave ablation <i>versus</i> resection for hepatocellular carcinoma within the Milan criteria: a 16 3.2 24 propensity-score analysis. Therapeutic Advances in Medical Oncology, 2019, 11, 175883591987465. Risk factors of intrahepatic biloma and secondary infection after thermal ablation for malignant 2.5 hepatic tumors. International Journal of Hyperthermia, 2019, 36, 979-984. MicroRNA-181a-5p and microRNA-181a-3p cooperatively restrict vascular inflammation and 18 6.3 91 atherosclerosis. Cell Death and Disease, 2019, 10, 365.

Kai Li

#	Article	IF	CITATIONS
19	Intraprocedural computed tomography/magnetic resonance–contrastâ€enhanced ultrasound fusion imaging improved thermal ablation effect of hepatocellular carcinoma: Comparison with conventional ultrasound. Hepatology Research, 2019, 49, 799-809.	3.4	11
20	Fusion imaging techniques and contrast-enhanced ultrasound for thermal ablation of hepatocellular carcinoma – A prospective randomized controlled trial. International Journal of Hyperthermia, 2019, 36, 1206-1214.	2.5	24
21	Inhibition of the mevalonate pathway enhances cancer cell oncolysis mediated by M1 virus. Nature Communications, 2018, 9, 1524.	12.8	21
22	Deficiency of the IRE1α-Autophagy Axis Enhances the Antitumor Effects of the Oncolytic Virus M1. Journal of Virology, 2018, 92, .	3.4	11
23	Automated breast tumor detection and segmentation with a novel computational framework of whole ultrasound images. Medical and Biological Engineering and Computing, 2018, 56, 183-199.	2.8	27
24	Selective Antagonism of Bcl-xL Potentiates M1 Oncolysis by Enhancing Mitochondrial Apoptosis. Human Gene Therapy, 2018, 29, 950-961.	2.7	13
25	Thermal ablation of hepatocellular carcinoma in patients with abnormal coagulation function. International Journal of Hyperthermia, 2018, 34, 1038-1043.	2.5	7
26	Immediate evaluation and guidance of liver cancer thermal ablation by three-dimensional ultrasound/contrast-enhanced ultrasound fusion imaging. International Journal of Hyperthermia, 2018, 34, 870-876.	2.5	54
27	Inhibition of Orai1-mediated Ca2+ entry limits endothelial cell inflammation by suppressing calcineurin-NFATc4 signaling pathway. Biochemical and Biophysical Research Communications, 2018, 495, 1864-1870.	2.1	13
28	Hexokinase 2â€dependent hyperglycolysis driving microglial activation contributes to ischemic brain injury. Journal of Neurochemistry, 2018, 144, 186-200.	3.9	80
29	Comparison of CT/MRI-CEUS and US-CEUS fusion imaging techniques in the assessment of the thermal ablation of liver tumors. International Journal of Hyperthermia, 2018, 35, 159-167.	2.5	28
30	DNA-PK inhibition synergizes with oncolytic virus M1 by inhibiting antiviral response and potentiating DNA damage. Nature Communications, 2018, 9, 4342.	12.8	38
31	Renal inhibition of miR-181a ameliorates 5-fluorouracil-induced mesangial cell apoptosis and nephrotoxicity. Cell Death and Disease, 2018, 9, 610.	6.3	33
32	Comparison of Transferred Deep Neural Networks in Ultrasonic Breast Masses Discrimination. BioMed Research International, 2018, 2018, 1-9.	1.9	107
33	The Anti-Warburg Effect Elicited by the cAMP-PGC1α Pathway Drives Differentiation of Glioblastoma Cells into Astrocytes. Cell Reports, 2017, 18, 468-481.	6.4	85
34	Targeting VCP enhances anticancer activity of oncolytic virus M1 in hepatocellular carcinoma. Science Translational Medicine, 2017, 9, .	12.4	55
35	Evaluation of the ablation margin of hepatocellular carcinoma using CEUS-CT/MR image fusion in a phantom model and in patients. BMC Cancer, 2017, 17, 61.	2.6	40
36	Improvement of ablative margins by the intraoperative use of CEUS-CT/MR image fusion in hepatocellular carcinoma. BMC Cancer, 2016, 16, 277.	2.6	40

Kai Li

#	Article	IF	CITATIONS
37	Naturally Existing Oncolytic Virus M1 Is Nonpathogenic for the Nonhuman Primates After Multiple Rounds of Repeated Intravenous Injections. Human Gene Therapy, 2016, 27, 700-711.	2.7	37
38	Activation of Cyclic Adenosine Monophosphate Pathway Increases the Sensitivity of Cancer Cells to the Oncolytic Virus M1. Molecular Therapy, 2016, 24, 156-165.	8.2	35
39	A classical PKA inhibitor increases the oncolytic effect of M1 virus via activation of exchange protein directly activated by cAMP 1. Oncotarget, 2016, 7, 48443-48455.	1.8	23
40	Transcriptional upregulation of microtubule-associated protein 2 is involved in the protein kinase A-induced decrease in the invasiveness of glioma cells. Neuro-Oncology, 2015, 17, 1578-1588.	1.2	21
41	Delayed bronchobiliary fistula and cholangiolithiasis following percutaneous radio frequency ablation for hepatocellular carcinoma. Experimental Biology and Medicine, 2015, 240, 156-159.	2.4	8
42	Genotyping of <i>Pneumocystis jirovecii</i> isolates from Chinese HIV-infected patients based on nucleotide sequence variations in the internal transcribed spacer regions of rRNA genes. Medical Mycology, 2013, 51, 108-112.	0.7	5
43	Absence of Pneumocystis jirovecii dihydropteroate synthase gene mutations among samples from a group of AIDS patients in China. Scandinavian Journal of Infectious Diseases, 2009, 41, 152-154.	1.5	12